

# Simulations of Adaptive Optics with a Laser Guide Star for SINFONI

Anthony G.A. Brown<sup>\*a</sup>, Enrico Fedrigo<sup>b</sup>, Paul van der Werf<sup>a</sup>

<sup>a</sup>Sterrewacht Leiden, P.O. Box 9513, 2300 RA Leiden, The Netherlands;

<sup>b</sup>European Southern Observatory, Karl-Schwarzschildstraße 2, D-85748 Garching bei München, Germany

## ABSTRACT

The SINFONI instrument for ESO's VLT combines integral field spectroscopy and adaptive optics (AO). We discuss detailed simulations of the adaptive optics module. These simulations are aimed at assessing the AO module performance, specifically for operations with extended sources and a laser guide star. Simulated point spread function (PSF) images will be used to support scientific preparations and the development of an exposure time calculator, while simulated wavefront sensor measurements will be used to study PSF reconstruction methods. We explain how the adaptive optics simulations work, focusing on the realistic modelling of the laser guide star for a curvature wavefront sensor. The predicted performance of the AO module is discussed, resulting in recommendations for the operation of the SINFONI AO module at the telescope.

## 1. INTRODUCTION

The SINFONI (SINGLE Far Object Near-ir Investigation) instrument is developed jointly by the European Southern Observatory, the Max-Planck-Institut für Extraterrestrische Physik, and the Netherlands Research School for Astronomy (NOVA). It combines integral field spectroscopy with adaptive optics in one instrument (see Refs. 1 and 2). The instrument will be available at ESO's VLT in 2004. The AO module of the instrument is based on a 60-element curvature wavefront sensor combined with a bimorph deformable mirror. The wavefront sensor employs 60 avalanche photo-diodes (APDs) as detectors. The AO system will operate in natural (NGS) and laser guide star (LGS) mode and will feed the corrected PSF to the near-infrared integral field spectrograph SPIFFI.<sup>2</sup>

As part of the NOVA contribution to this project detailed simulations of an AO system with a curvature sensor, tailored to the details of the SINFONI AO module, are being carried out. The aim is to develop a realistic simulation of the operation of the AO module with a laser guide star generated in the mesospheric sodium layer. The output consists of detailed statistics of the AO system performance as well as PSF images (at  $J$ ,  $H$ , and  $K$ -band) and wavefront sensor data. The results will be used to support the development of algorithms for PSF reconstruction from wavefront sensor data (see Ref. 3 in this volume) and the development of an exposure time calculator. Scientific preparations for the use of the SINFONI instrument will also be supported with these simulations.

## 2. OVERVIEW OF THE BASIC SINFONI AO SIMULATION TOOL

The simulation code is based on a Matlab adaptive optics plus curvature wavefront sensor simulation package developed at ESO.<sup>4</sup> The basic structure of the simulated AO system as well as the light and signal paths are shown in Fig. 1. The atmospheric turbulence is simulated with three phase screens to which a height, weight, and wind speed can be assigned. The phase structure function simulated by the phase screens follows a Kolmogorov spectrum and the screens are normalised such that unit phase variance (1 radian<sup>2</sup>) is attained over a circular region of 128 samples in diameter. The screens can thus be normalised for any value of the Fried parameter  $r_0$  by scaling with  $\sqrt{1.03(D/r_0)^{5/3}}$ , where  $D$  is the diameter of the telescope primary mirror, which is sampled by 128 samples. The simulations discussed below use a value of  $r_0 = 16$  cm, which corresponds to a seeing of 0.65 arcsec at an observing wavelength of 550 nm.

---

\*brown@strw.leidenuniv.nl

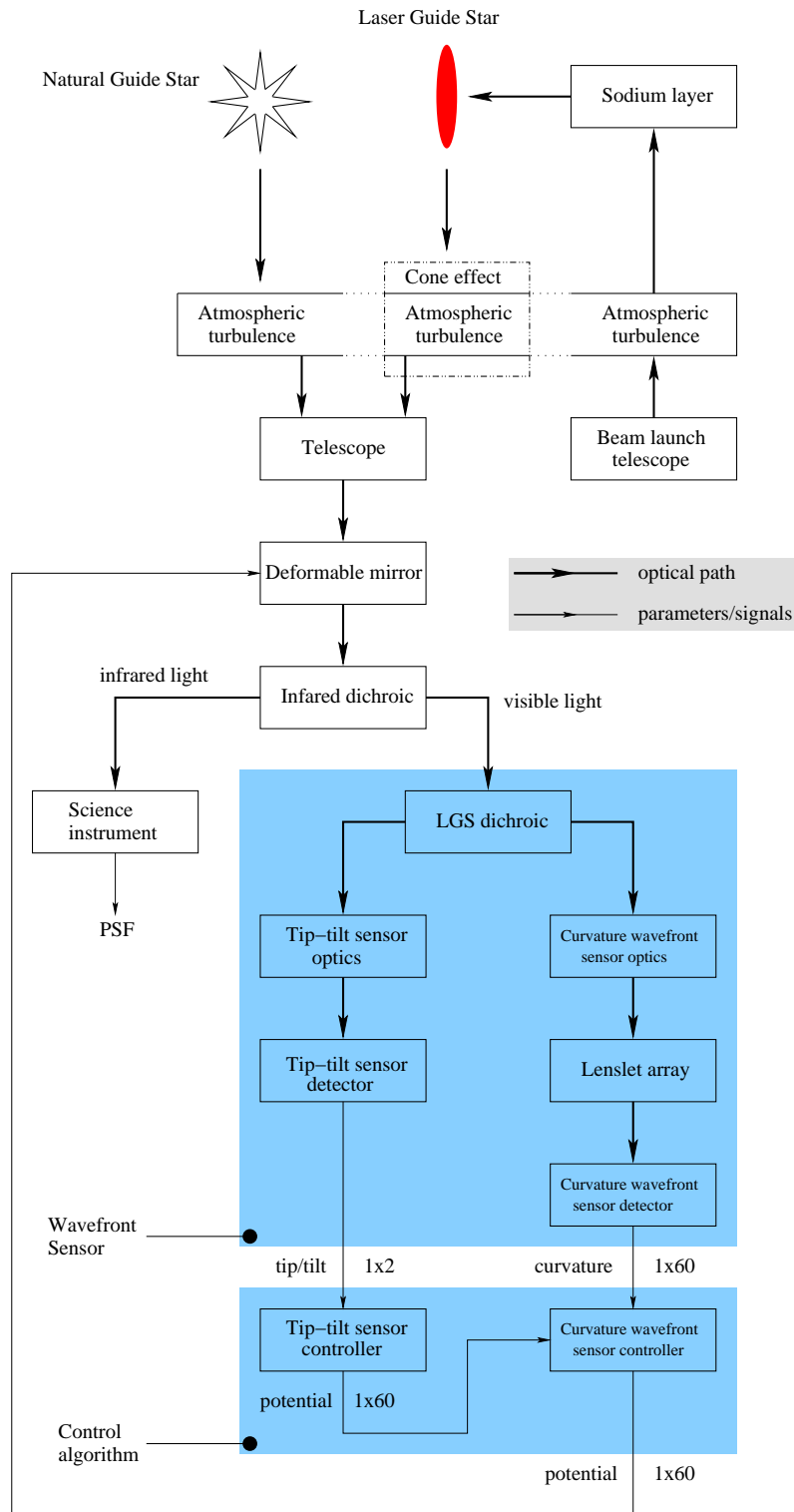


**Figure 1.** Structure of the AO simulation package. The figure is after Ref. 4 (Fig. 4.1) with the addition of the laser guide star parts. This includes the cone effect for the LGS and the presence of a natural guide star for tip-tilt sensing.

The AO corrections are done with a deformable mirror (DM) which is simulated through a detailed finite-element model of the bimorph mirror that will be used in the real system. The curvature wavefront sensor optics module implements the membrane mirror as a time-varying focus term that is added to the phase of the optical field. The lenslet array module divides the light among the 60 elements of this array and the light is then detected with simulated APDs by the detector module. The simulations include the variation of the field of view of the lenslet array with the membrane mirror focal length. This is implemented as a vignetting of the optical field after reflection off the membrane mirror. The curvature signal is constructed as the difference of the accumulated intra- and extra-focal intensity distributions and sent to the controller module which steers the DM. For LGS operation an additional tip-tilt (TT) sensor is needed which is modelled as a simple quad-cell.

For propagating the light through the system the Fraunhofer approximation is used everywhere, which implies a Fourier transform at each propagation from a pupil to an image plane or vice versa.

At the start of the simulation the interaction matrix between the curvature sensor and the DM is determined by applying voltages to each actuator of the DM in turn and then measuring the resulting curvature signal. The control matrix is the pseudo inverse of the interaction matrix, which is obtained after filtering out the smallest eigenvectors from the latter.

The basic AO simulation package developed at ESO only handled the case of a natural guide star (i.e. a point source outside the atmosphere) and was extended to include a laser guide star. The beacon produced by the laser guide star facility in the sodium layer will be a three-dimensional region from which photons are returned to the telescope. The AO simulation thus has to model how the beacon is generated and how the curvature sensor ‘sees’ a 3D light distribution, extended along the line of sight. In the case of the VLT the laser light will be launched from behind the secondary mirror which means that the laser beacon is always on axis. This allows the modelling of the beacon as a stack of extended (2D) sources (see Sect. 4). The first extension of the AO simulation tool was thus to include extended (natural) guide sources which is described in the following section. This has an interest of its own as in reality there are many occasions where one may want to guide the AO system on an extended source. In Sect. 4 a detailed description is given of the subsequent implementation of the laser guide star.

### 3. IMPLEMENTING AN EXTENDED NATURAL GUIDE SOURCE

The extended guide source (EGS) was implemented in the simulations by considering it to be a collection of independent point sources at different positions on the sky that all contribute to the extended source signal. It is assumed that the light from each point source travels along the same path through the atmosphere (i.e., anisoplanatism effects over the extent of the source are neglected). The light of these point sources will travel from the VLT primary mirror to the curvature wavefront sensor and there reflect off the membrane mirror which is located in the focal plane of the telescope. After reflection the light goes on to the lenslet array where for a flat membrane a replica of the VLT entrance pupil (the pupil image) is formed.

For a flat membrane mirror the pupil image at the lenslet array will be a uniformly illuminated disk (with a hole in the middle caused by the VLT secondary). When the membrane mirror is curved a defocus term is added to the optical field reflecting off the mirror which results in a pupil image at the lenslet array that contains information on the phase structure of the optical field at the VLT primary (this is the basis for the functioning of a curvature sensor). In the presence of a pure tilt in the phase of the optical field at the VLT pupil, the defocus term leads to a shift of the pupil image on the lenslet array.

This means that for a collection of point sources on the sky the resulting image will be the convolution of the pupil image for an on-axis point source with the distribution of point sources (i.e. the extended source intensity distribution) on the sky. In order to implement this correctly in the simulations it is necessary to know how the angular scale on the sky translates to the linear scale at the lenslet array. This can be derived from a Fourier analysis of the path that the light takes from the VLT pupil to the lenslet array. It can be shown that in the presence of a pure tilt in the wavefront the pupil image only undergoes a shift  $\Delta s$  (in mm) which is given by:

$$\Delta s = \tau \frac{(f - f_m)}{f_m} f_L \approx \tau \frac{f f_L}{f_m} = \frac{\zeta}{f_m} \tau, \quad (1)$$

**Table 1.** Parameters of the AO simulations with a natural guide source which can be a point source or extended. The column on the left lists the parameters that can be varied during the simulations and the column on the right shows the default value, or range of values, used in the simulations.

Model parameter	Value
Overall	
Seeing	0.65 arcsec at 500 nm
NGS/EGS wavelength	700 nm
NGS/EGS magnitude	9–16
NGS/EGS size	0–2 arcsec FWHM (Gaussian light distribution)
Sky background magnitude	19
Science wavelength	$J, H, K$
Integration time	1 second
Position of NGS/EGS and science target	Both on-axis and at zenith
Telescope focal length	374.4 m
Wavefront sensor	
Membrane mirror focal length	10–100 cm
Membrane mirror frequency	2100 Hz
Time step	29.8 micro-seconds (16 samples per membrane period)
Atmosphere update interval	238 micro-seconds (8 time steps)
Curvature sensor loop gain	0.1–0.9
Curvature sensor integration periods	6
APD read-out delay	0 seconds
APD read-out noise	0 e <sup>-</sup>
APD curvature sensor quantum eff.	0.70
APD curvature sensor dark current	250 e <sup>-</sup> /sec
APD tip-tilt sensor quantum eff.	0.70
APD tip-tilt sensor dark current	250 e <sup>-</sup> /sec

where  $\tau$  is the angular distance from the optical axis (in arcseconds on the sky),  $f$  is the focal length of the beam coming from the primary mirror,  $f_m$  is the membrane mirror focal length\*, and  $f_L$  is the focal length of the beam travelling from the membrane mirror to the lenslet array. The approximation on the right is valid to within 2 per cent for the range of values of  $f_m$  occurring in practice. In the simulations we use  $\zeta = 1220 \text{ mm}^2/\text{arcsec}$  ( $f_m$  in mm and  $\tau$  in arcsec).

### 3.1. Predicted performance for natural guide sources

Having implemented an extended natural guide source in the simulations we can now use them to predict the performance on such sources and compare that to the performance for point sources. The extended sources can in reality have arbitrary intensity distributions on the sky but we only investigated Gaussian light distributions for a range of FWHM values. The parameters of the simulation that can be tuned are listed in Table 1.

The simulations were used to investigate how the performance of the AO system, as measured by the Strehl ratio of the PSF, varies as a function of the brightness and size of the guide source, the membrane mirror focal length and the curvature sensor control-loop gain. The results can be used during actual operations of the AO system to guide the optimisation of the settings.

The resulting performance figures for a control loop gain of 0.6 (which is close to optimal in most cases) are shown for the  $J, H,$  and  $K$  bands in Figs. 2–4. Figure 2 shows how the performance varies as a function of the membrane mirror focal length for various source sizes and magnitudes. Figures 3 and 4 show the Strehl ratio

\*The focal length of the membrane mirror will be used throughout this paper instead of the more common radius of curvature (which is twice the focal length).

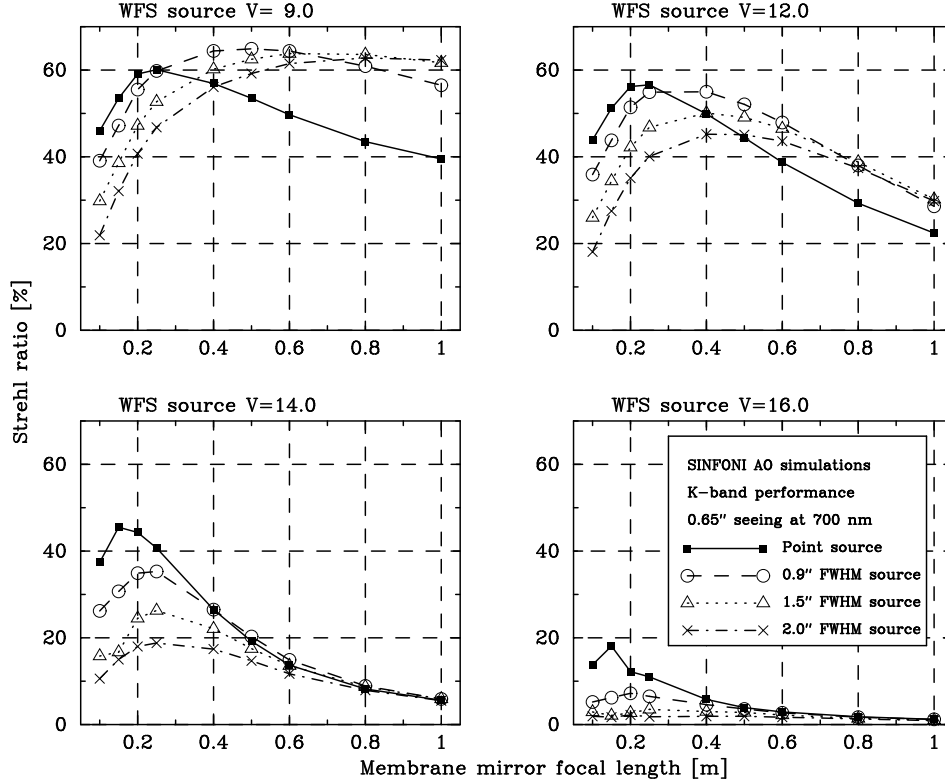


**Figure 2.** The four diagrams show the performance of the SINFONI AO module for natural guide sources at  $K$ -band. The light distribution of the extended sources is Gaussian. The Strehl ratio of the PSF is measured after 1 second of integration time. The four panels are for different magnitudes of the guide source ( $V = 9, 12, 14, 16$ ) and the Strehl ratios are shown for different source sizes (0, 0.9, 1.5, and 2.0 arcsec FWHM; as measured on the sky outside the atmosphere) as a function of the focal length of the membrane mirror of the curvature sensor.

and 50% encircled energy radius at each magnitude after the membrane mirror focal length has been adjusted to its optimal value.

From considerations of the characteristics of curvature based systems (see Ref. 5, Sect. 5.3.3) it is expected that for extended guide sources one should increase the extra-focal distance realised with the membrane mirror (i.e., increase the mirror focal length or, equivalently, reduce the stroke of the membrane) in order to optimise the performance. However, the sensitivity of the system decreases with larger extra-focal distances so some compromise between membrane stroke and source brightness is expected to optimise the performance for the EGS case.

This is confirmed by the results obtained from the simulation of the SINFONI AO module. Inspection of Fig. 2 shows a general trend that for a given source magnitude (for the brighter sources) the performance reaches its optimum for longer extra-focal distances as the source size increases. On the other hand, for a given guide source size the optimum performance shifts toward smaller extra-focal distances as the source brightness decreases (the same behaviour is seen for  $J$  and  $H$ ).

However for the brightest guide sources the optimum performance for the extended sources is always better than the optimum performance for the point source (as judged by the Strehl ratio and the 50% encircled energy radius). Intuitively one expects that no matter how well optimised the EGS case is, information is always lost due to the smearing out of the signal. However this smoothing of the signal also leads to the filtering out of the high frequency spatial aliasing that occurs in curvature wavefront sensors. This improves the performance at high signal-to-noise ratios (F. Rigaut, priv. communication).

For operating the SINFONI AO module on natural guide sources the following recommendations can be made

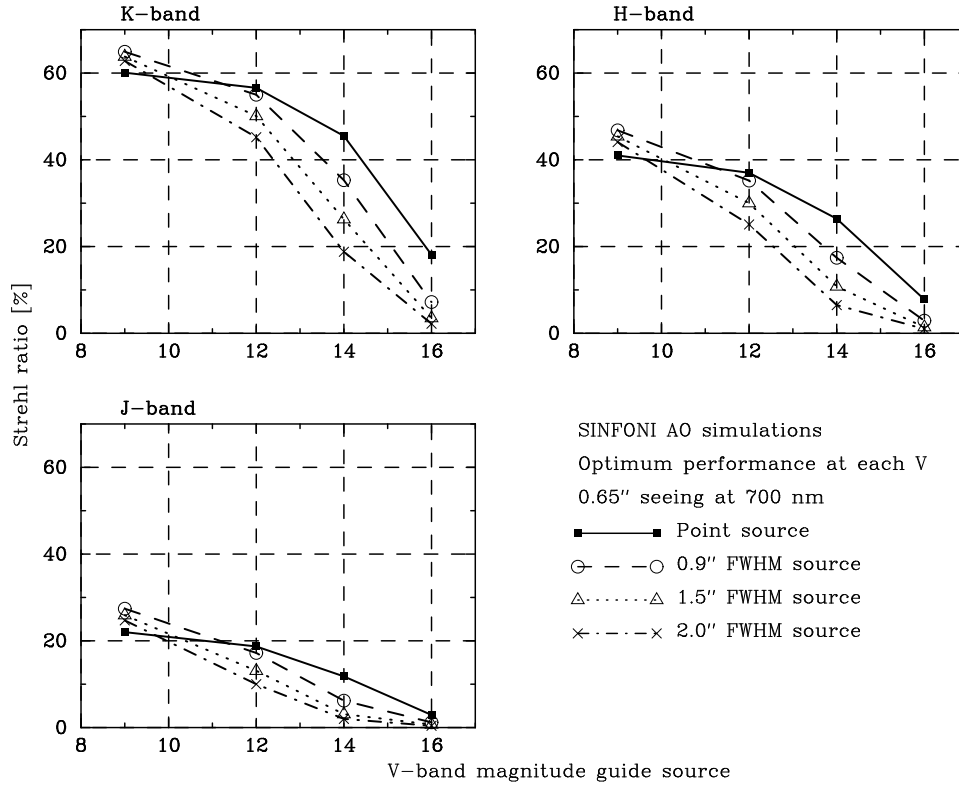


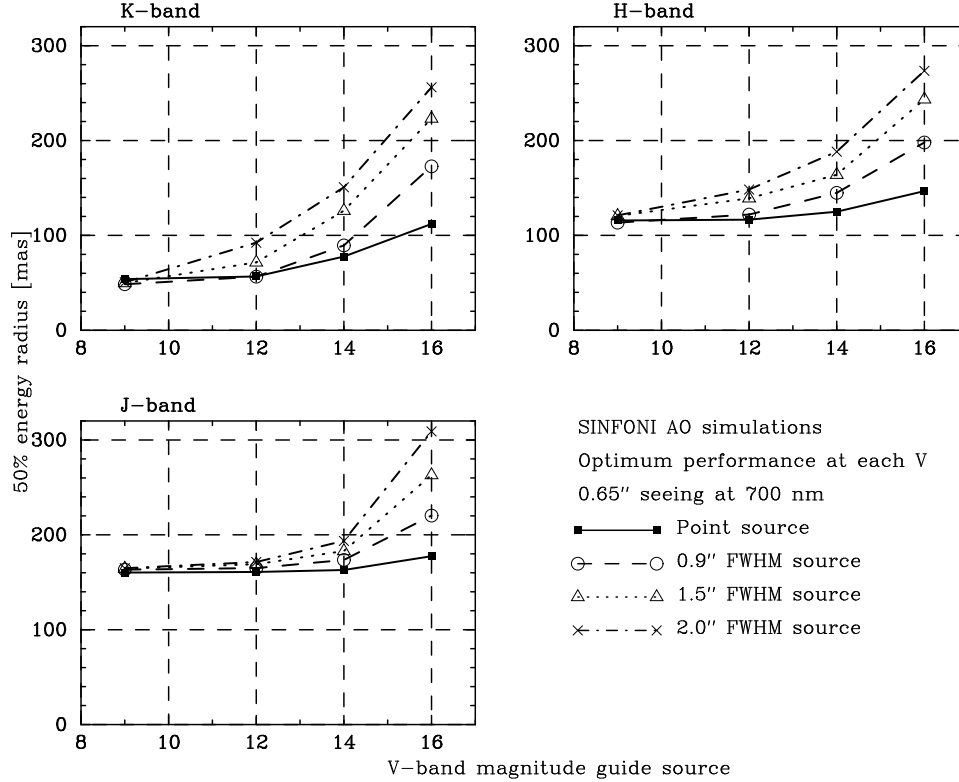
**Figure 3.** The performance of the AO system for the *J*, *H*, and *K*-bands as measured by the Strehl ratio. The performance at each magnitude was optimised by varying the membrane mirror focal length (see Fig. 2).

based on the simulation results: For point sources brighter than  $V \sim 14$  the optimum membrane mirror focal length is  $\sim 0.25$  m. This value should be lowered to 0.1–0.2 m for fainter sources. For extended sources brighter than  $V \sim 14$  the membrane mirror focal length should be adjusted during the operation of the AO system in order to improve performance. For extended guide sources fainter than  $V \sim 14$  the membrane mirror focal length should be kept at about 0.25 m. Experiments with the simulations show that a re-calibration of the interaction matrix for extended sources (by calibrating on an artificial extended source) does not improve the performance and thus is not necessary. The calibration can always be done on a point source.

#### 4. IMPLEMENTING THE LASER GUIDE STAR

The laser guide star facility that will be installed at ESO’s VLT will make use of the mesospheric sodium layer to produce the laser beacon. The telescope that will launch the laser light will be located behind the secondary mirror of the VLT, resulting in a monostatic projection (i.e. on-axis with respect to the primary mirror).<sup>6</sup> Figure 5 shows a schematic diagram of this situation. The laser beam is launched by the beam launch telescope (BLT) and travels upwards to the sodium layer, spreads out along the way due to diffraction, and suffers the effects of turbulence. In the sodium layer the laser light is resonantly back-scattered and this results in a laser beacon which because of the finite width of the layer is extended in 3 dimensions<sup>†</sup>. Subsequently the laser light travels back down to the telescope, again going through turbulence, whereafter it will be analysed by the AO system. Turbulent layers at different heights are present and the sodium layer is located a height  $z_0$  and has a thickness  $L$ .

<sup>†</sup>Note: the 3D distribution of back-scattered laser light in the sodium layer will be referred to as the laser ‘beacon’, whereas the image of this beacon as seen from the ground will be referred to as the laser ‘spot’.



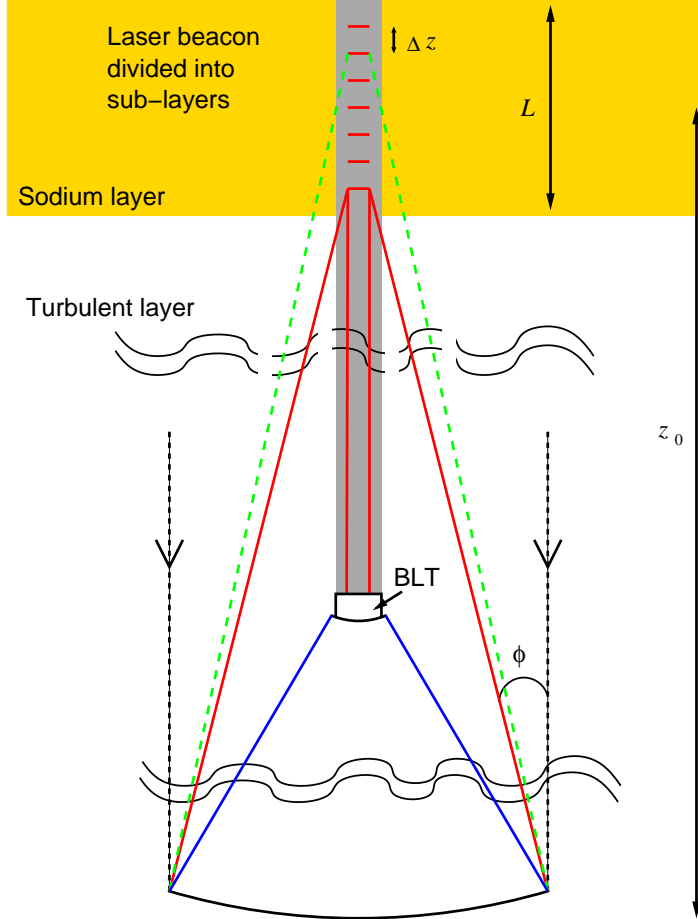
**Figure 4.** Optimum performance of the AO system at *J*, *H*, and *K* as measured by the 50% encircled energy radius (in units of milli-arcseconds).

Figure 5 also shows how the laser beacon is actually modelled in the simulation. It is represented as a stack of 2D extended sources. For each of these one needs to know the height, the number of photons returned, and the distribution of photons in the 2D spot before downward propagation of the laser light. The laser beam optical field at launch is assumed to have a constant phase which upon propagation to the sodium layer will be affected by turbulence. The resulting intensity distribution in the sodium layer corresponds to the image of the 2D sources unaffected by turbulence from the downward path. Finally, the light from each 2D source will propagate back to the telescope and pass through turbulence layers and now the cone effect and loss of tip-tilt information in the laser signal have to be taken into account.

#### 4.1. Laser beam launch and upward propagation

The beam launch telescope will have a primary mirror of 50 cm (clear aperture outer diameter) and a central obscuration of 4.2 cm. The profile of the laser beam can be taken to be a Gaussian (i.e., the optical field has an amplitude which has a Gaussian shape perpendicular to the beam direction). The launched  $1/e^2$  diameter of the laser beam will be 35 cm.<sup>6</sup> The BLT is assumed to be focused at the altitude of the centroid of the sodium layer and then the irradiance distribution at that point due to the laser light can be obtained by a Fourier transform of the laser optical field. The FWHM size of this spot in the absence of turbulence will be about 0.29 arcseconds for the VLT laser guide star facility. The presence of atmospheric turbulence on the way up to the sodium layer is taken into account by adding the phase from the atmospheric phase screens to the optical field of the laser beam. The atmospheric phase screens are represented by a  $128 \times 128$  matrix over the size of the VLT pupil (8 m) and the inner  $8 \times 8$  samples (the  $50 \times 50$  cm<sup>2</sup> region seen by the BLT) of the phase screens are used to simulate the effect of turbulence on the laser beacon. The cone effect on the upward path is ignored in the simulations.

After Fourier transforming the laser optical field including the turbulence one obtains the intensity distribution of the 2D sources that represent the laser spot. Just as for the extended natural guide sources (Sect. 3) this



**Figure 5.** Schematic diagram of the simulation of a laser guide star for SINFONI. The sodium layer is divided into sub-layers that are considered to be so thin that the resulting back-scattered photons come from a 2D region. Thus the LGS is simulated as a stack of extended 2D guide sources. For each EGS one has to calculate its light distribution and the location where it will be focused. The response of the curvature sensor to the separate EGS's can then be summed to obtain the LGS response. The differential cone effect, illustrated here by the two cones coming down from different layers in the laser beacon, can be ignored in the SINFONI simulations.

intensity distribution is convolved with the point source pupil image at the lenslet array of the curvature sensor. In this way the 2D extent of the laser guide star across the line of sight is taken into account.

The diameter of the BLT spans only a few turbulence ‘cells’ of size  $r_0$  (i.e.,  $D/r_0 \sim \text{few}$ ). This implies a high Strehl ratio for short exposure images of the laser spot, making the spot size not much larger than the 0.29 arcseconds quoted above. Note that this refers to the spot size *before* downward propagation.

## 4.2. Laser beacon generation

This part of the simulation code takes care of generating a realistic distribution of the returned photons as a function of the location within the 3D laser beacon. The theory of photon return from sodium beacons is extensively discussed in two papers by Milonni and co-workers<sup>7,8</sup> and their results are used in the calculations of the photon return rate in the simulation. For a continuous-wave laser as used for the VLT the photon return per unit area at the receiver can be written as:

$$R_{\text{cw}} \propto \frac{T_0 C_S}{z_0^2}, \quad (2)$$



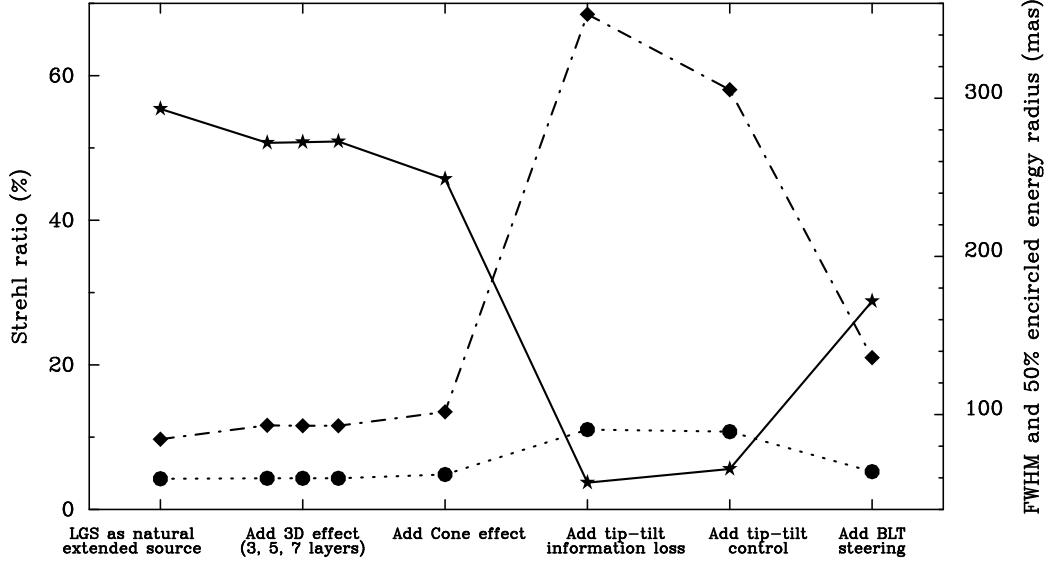


**Figure 6.** The effects of increasing the realism of the laser guide star simulations. The plot shows the Strehl ratio (starred symbols, left vertical scale), the full-width half-maximum and the 50% encircled energy radius (in milli-arcseconds, filled circles and diamonds respectively, right vertical scale) of the PSF at K-band after 1 second of integration time. From left to right the realism of the simulations is increased by adding the effects listed on the horizontal axis.

where the constants are the atmospheric transmission  $T_0$ , the sodium atom column density  $C_S$ , and the height of the sodium layer  $z_0$ . Note that the atmospheric transmission only contains the downward component. In reality one deals with an overall transmission  $\eta T_0^2$ , where  $T_0$  occurs twice to account for the up and down propagation of the laser beam and the factor  $\eta$  includes the transmission coefficients of the beam transportation system, the beam launch telescope, and the astronomical (VLT-UT) telescope.

When dividing the laser beacon into discrete 2D sources Eq.(2) can be used to calculate for each 2D source the relative number of photons (with respect to the sodium centroid altitude) returned to the curvature sensor. Dividing the sodium layer into  $n$  discrete layers of thickness  $\Delta z$ , the column density can be obtained by integrating of the vertical sodium density distribution  $\rho(z)$  and the atmospheric transmission can be calculated relative to the transmission corresponding to the sodium centroid altitude. The number of photons  $N_{\text{ph},i}$  returned from each sub-layer  $i$  is given by:

$$N_{\text{ph},i} = N_{\text{ph}} \frac{w_i}{\sum_i w_i} \quad \text{and} \quad w_i = \left( \frac{z_0}{z_i} \right)^2 e^{\frac{2 \ln T_0}{z_0} (z_i - z_0)} \int_{z_i - \frac{\Delta z}{2}}^{z_i + \frac{\Delta z}{2}} \rho(z) dz, \quad (3)$$

where  $N_{\text{ph}}$  is the total number of photons (summed over the sub-layers),  $z_i$  is the centroid altitude of sub-layer  $i$ , which has a thickness  $\Delta z$ . The first factor in the calculation of  $w_i$  takes the geometrical dilution of the photon return into account, the second factor describes the atmospheric transmission, and the third factor is the column density for sub-layer  $i$ . The relative transmission is calculated assuming that the optical depth is proportional to  $z$ . The factor 2 in the exponential takes into account the upward and downward path of the laser light through the atmosphere (the extra transmission factor  $\eta$  mentioned above is the same for all sub-layers and need not be explicitly known for this calculation). The density  $\rho(z)$  is assumed to be a Gaussian with a full width half maximum equal to the thickness  $L$  of the sodium layer. Note that the geometrical dilution and transmission factors should be included in the integral but have been approximated here by their values at the distance  $z_i$  of each sub-layer  $i$ .

### 4.3. Downward propagation and the cone effect

On downward propagation of the laser light the atmosphere will not be fully sampled. The atmosphere above the LGS is not seen at all and below the LGS only the atmosphere within a cone of opening angle  $2\phi$  will be

**Table 2.** Parameters of the AO simulations with a laser guide star. These parameters are used in addition to those listed in Table 1. The column on the left lists the parameters that can be varied during the simulations and the column on the right shows the default value, or range of values, used in the simulations. (SCA stands for sodium centroid altitude.)

Model parameter	Value
Laser beacon and tip-tilt star	
LGS wavelength	589 nm
NGS (tip-tilt star) wavelength	700 nm
Position of LGS beacon and science target	Both on-axis
Return flux from LGS	$10^6$ photons/sec/m <sup>2</sup>
Atmospheric transmission up to SCA	0.7
Laser beam launch	On axis
Beam launch telescope diameter	50 cm; focused to SCA
Laser beam	Gaussian; $1/e^2$ -diameter 35 cm
Sodium layer	Height 90 km asl, thickness 3–10 km, Gaussian density distrib.
No. of layers in sodium beacon model	3
Telescope altitude	2635 m asl
SCA measurement error	0–few hundred m
LGS zenith angle	0–60 degrees
TT (tip-tilt) star magnitude	12–18
TT star offset from LGS	0–60 arcsec
TT star position angle wrt LGS	0–360 degrees
Control loops	
Tip-tilt sensor integration periods	6
TT sensor loop gain	9
BLT steering mirror loop gain	2.2
BLT steering mirror time delay	0– $N$ time-steps
Atmosphere	
Layer heights	0, 7000, 13000 meter
Layer weights	0.6, 0.2, 0.2
Layer speeds	5.7, 5.7, 33.0 meter/sec

seen (see Fig. 5). For an 8 m telescope and a height of the LGS of 90 km,  $2\phi \sim 9 \times 10^{-5}$  rad. This means for example that of a turbulent layer at a height of 10 km only a circle of 7.1 m diameter will be seen. There is also a differential cone effect due to the extent of the laser beacon along the line of sight (see Fig. 5). This means that light coming from the bottom and top of the laser beacon arriving at the same position on the telescope primary mirror will have travelled at slightly different angles through the turbulence, thus causing a differential anisoplanatism error. For the SINFONI case this can be ignored as the additional information smearing occurs on scales of a few tens of centimetres which is much smaller than the resolution elements of the curvature sensor across the primary mirror (which are of order 1 meter).

For downward propagation the cone effect is taken into account by calculating for each turbulent atmosphere layer what fraction of the  $8 \times 8$  m phase screen ( $128 \times 128$  samples across the VLT pupil) is seen from the sodium layer. The resulting  $n \times n$  ( $n < 128$ ) sample phase screen is scaled to  $128 \times 128$  samples. All the resulting phase screens from each turbulent layer are then added to obtain the overall effect on the laser beacon. The response at the curvature sensor is calculated for each sub-layer making use of the 2D intensity distribution which is obtained as explained in Sect. 4.1.

#### 4.4. 3D effect at the curvature sensor

The different 2D sources in the stack that simulates the laser beacon are not all located at the sodium centroid altitude to which the AO system is focused. This means that the layers away from the sodium centroid altitude

will be seen out of focus at the curvature sensor. Equivalently one can think in terms of the outer parts of the curvature sensor lenslet array seeing an elongated laser spot. The effect of the 3D extent of the laser beacon is a radial smearing of the information at the lenslet array. This effect is implemented as an additional focus term that is added to the optical phase for each sub-layer  $i$ , which is proportional to  $(1/z_i - 1/z_0) \times (\xi^2 + \eta^2)$ , where  $(\xi, \eta)$  are the coordinates across the VLT pupil. After the response of the curvature sensor to each individual sub-layer  $i$  is calculated all the signals are added to obtain the overall response.

#### 4.5. Tip-tilt management

One of the most important issues when using laser guide stars is that of the tip-tilt corrections to be applied to the wavefront corresponding to the scientific target. The laser light launched from the BLT will suffer the effects of turbulence on both the upward and downward paths leading to a summed tip-tilt component in the laser light phase that is different from and uncorrelated with the tip-tilt component in the phase of the light from the science target. This necessitates the addition of a natural guide star for tip-tilt sensing (the ‘tip-tilt star’) in order to correct the tip-tilt of the science target wavefront. The tip-tilt star will in general be located away from the science target which leads to tilt-anisoplanatism errors in the corrected wavefront. We now describe how these issues are accounted for in the simulations.

In the simulations the tip-tilt components of the atmospheric phase screen seen by the BLT are saved and then subtracted from the phase screen to be used for downward propagation (after multiplication of the tip-tilt coefficients by the ratio of the VLT to BLT pupil). This correctly simulates how the tip-tilt motion of the laser beacon is affected by up- and down propagation of the laser light.

A separate tip-tilt sensor is implemented in the simulations as a simple quad-cell detector which senses the wavefront from a natural guide star. In the SINFONI AO module the tip-tilt compensation of the science wavefront will be done with the deformable mirror which is inserted in a tip-tilt mount. The deformable mirror will thus be steered by both the curvature and the tip-tilt sensor so one has to take care in not having the tip-tilt signal contained in the laser light interfere with the tip-tilt steering. This is implemented in the simulation by removing from the curvature controller potential vector the part corresponding to a flat mirror surface and replacing that by the potential vector from the tip-tilt controller.

The tip-tilt signal at the curvature sensor due to the laser guide star will be large if the position of the LGS on the sky is not stabilised. This will then drive the curvature signal into the non-linear regime and render the higher order corrections invalid. Thus the LGS itself also has to be stabilised which will be done by a steering mirror inserted into the light path at beam launch. The required tip-tilt compensation is contained in the tip-tilt signal measured in the laser light by the curvature sensor. The latter signal is used in the simulations to control the steering mirror of the BLT.

#### 4.6. Additional simulation elements

A number of options have been added to the simulation package to facilitate the study of the AO system performance under varying observing conditions. The height and thickness of the sodium layer can be varied and a constant focus error can be added (which simulates a telescope focused at the wrong height). In addition observations can be simulated away from zenith and the natural guide star for tip-tilt sensing can be placed off-axis to simulate tilt-anisoplanatism effects. All parameters of the LGS components of the simulation are listed in Table 2.

### 5. LGS SIMULATION RESULTS

After putting together all the LGS simulation elements described in the previous section one can investigate the performance predicted for the SINFONI AO system used with a laser guide star. Figure 6 shows the performance of the simulated SINFONI AO system as the realism of the simulations is increased. The membrane mirror focal length was 25 cm in these simulations. The three lines show for 1 second of integration time; the Strehl ratio (line with starred symbols, scale on the left), the FWHM (line with dots, scale on the right) and the 50% encircled energy radius (line with diamonds, scale on the right). The leftmost points show the performance if one would take the 2D laser spot corresponding to an infinitesimally thin sodium layer and put it outside the atmosphere.

Thus the performance with respect to a point source is only degraded by the source extent on the sky. From left to right the realism of the simulations is increased by adding first the 3D-effect (using 3, 5, and 7 layers for the laser beacon), then the cone-effect, and finally the effects of the loss of tip-tilt information in the laser light.

These results show that the 3D light distribution of the LGS beacon is already well modelled by three sub-layers. The combination of the 3D and cone effects lead to a  $\sim 10\%$  loss in Strehl ratio (starting from 55%). Note the dramatic performance loss once the tip-tilt complications are included. The addition of a tip-tilt star does not improve the performance unless at the same time the launched laser beam is stabilised on the sky. The performance for the latter case corresponds to a Strehl ratio of 29%. This can be further optimised by changing the membrane mirror focal length to 40 cm and tuning the gains of the three control loops. The optimum performance achieved is then 36% at K-band.

## 6. CONCLUSIONS AND FUTURE WORK

We have described detailed simulations of the SINFONI AO module and used these to make performance predictions for operation with natural (extended) guide sources and a laser guide star. The results can be used to guide the optimisation of the AO module settings during actual observations (see Sect. 3.1) and to support other activities such as the study of the reconstruction of the PSF from wavefront sensor data and the scientific preparation of observations with SINFONI.

Concerning the laser guide star mode a number of tasks and open issues remain. The predicted performance of the laser guide star mode of the SINFONI AO module will be mapped as a function of various parameters, such as the tip-tilt star brightness and distance from the science target, the zenith angle, the characteristics of the sodium layer, and the natural seeing. The steering of the BLT mirror is currently done in open loop in the simulations and is quite sensitive to the exact gain settings for the three control loops present in the AO module. The LGS performance can possibly be improved further by switching to closed loop control of the BLT steering mirror and further investigating how the different control loops interact and how their gains should be optimised.

## ACKNOWLEDGMENTS

We thank Rudolf Le Poole, Miska Le Louarn, Enrico Marchetti and Markus Kasper for fruitful discussions that greatly helped along the development of the simulations at various stages.

## REFERENCES

1. H. Bonnet et al., “Implementation of MACAO for SINFONI at the VLT, in NGS and LGS modes,” in *Adaptive Optical System Technologies II. Edited by Wizinowich, Peter L.; Bonaccini, Domenico. Proceedings of the SPIE, Volume 4839*, pp. 329–343, 2003.
2. F. Eisenhauer et al., “SINFONI - Integral field spectroscopy at 50 milli-arcsecond resolution with the ESO VLT,” in *Instrument Design and Performance for Optical/Infrared Ground-based Telescopes. Edited by Iye, Masanori; Moorwood, Alan F. M. Proceedings of the SPIE, Volume 4841*, pp. 1548–1561, 2003.
3. F. Rigal, P. van der Werf, and E. Fedrigo, “Reconstruction of the long-exposure point spread function of the VLT SINFONI/MACAO system using control loop data,” this Proceedings.
4. T. V. Craven-Bartle, “Modelling curvature wavefront sensors in adaptive optics,” Master’s thesis, Linköping University, 2000.
5. G. Rousset, “Wave-front sensors,” in *Adaptive Optics in Astronomy*, F. Roddier, ed., pp. 91–130, Cambridge University Press, 1999.
6. D. Bonaccini et al., “VLT laser guide star facility,” in *Adaptive Optical System Technologies II. Edited by Wizinowich, Peter L.; Bonaccini, Domenico. Proceedings of the SPIE, Volume 4839*, pp. 381–392, 2003.
7. P. W. Milonni, R. Q. Fugate, and J. M. Telle, “Analysis of measured photon returns from sodium beacons,” *Optical Society of America Journal* **15**, pp. 217–233, 1998.
8. P. W. Milonni, H. Fearn, J. M. Telle, and R. Q. Fugate, “Theory of continuous-wave excitation of the sodium beacon,” *Optical Society of America Journal* **16**, pp. 2555–2566, 1999.